JVSTB Journal of Vacuum Science & Technology B

# Structural and electrical investigation of laser annealed ( Pb , Sr ) Ti O 3 thin films

Jyh-Liang Wang, Yi-Sheng Lai, Sz-Chian Liou, Bi-Shiou Chiou, Chueh-Kuei Jan, and Huang-Chung Cheng

Citation: Journal of Vacuum Science & Technology B **26**, 41 (2008); doi: 10.1116/1.2819255
View online: http://dx.doi.org/10.1116/1.2819255
View Table of Contents: http://scitation.aip.org/content/avs/journal/jvstb/26/1?ver=pdfcov
Published by the AVS: Science & Technology of Materials, Interfaces, and Processing

# Structural and electrical investigation of laser annealed $(Pb,Sr)TiO_3$ thin films

Jyh-Liang Wang
*Department of Electronics Engineering and Institute of Electronics, National Chiao Tung University, 1001 Ta Hsueh Rd., Hsinchu 30050, Taiwan*

Yi-Sheng Lai[a)]
*Department of Materials Science and Engineering, National United University, Miaoli 36003, Taiwan*

Sz-Chian Liou
*Center for Condensed Matter Sciences, National Taiwan University, Taipei 10617, Taiwan*

Bi-Shiou Chiou, Chueh-Kuei Jan, and Huang-Chung Cheng
*Department of Electronics Engineering and Institute of Electronics, National Chiao Tung University, 1001 Ta Hsueh Rd., Hsinchu 30050, Taiwan*

(Received 16 July 2007; accepted 5 November 2007; published 2 January 2008)

Material and electrical characteristics of $(Pb,Sr)TiO_3$ (PSrT) films irradiated by various laser pulses and laser fluences are investigated in this work. Enhanced crystallinity can be obtained after excimer laser annealing (ELA). However, grain growth induced by ELA is nonuniform, and the effect is limited to the upper region of the films. As the number of laser pulses increases to 120, the film shows stronger diffraction intensities and increased oxygen content, resulting in a distinct capacitance versus electric field hysteresis loop and a larger dielectric constant than the nonirradiated one. The leakage current is found to be associated with the interface quality. The conduction mechanism of nonirradiated and irradiated PSrT films is mainly governed by Schottky emission at low electric fields, whereas the Poole-Frenkel emission occurs for films irradiated with more than 120 laser pulses or laser fluences larger than 90.5 $mJ/cm^2$ at high electric fields. © *2008 American Vacuum Society.* [DOI: 10.1116/1.2819255]

## I. INTRODUCTION

$(Pb,Sr)TiO_3$ (PSrT) films, with perovskite structure, have received much attention lately due to their potential applications in memory, sensor, and microwave devices.[1–6] The PSrT film constitutes a solid solution of $PbTiO_3$ (PTO) and $SrTiO_3$ (STO). PTO exhibits ferroelectric transition at the Curie temperature of 490 °C, whereas STO exhibits no ferroelectric phase transition, but undergoes structural phase transition from cubic to tetragonal symmetry around −168 °C (105 K).[7] Therefore, PTO and STO films, at room temperature, have tetragonal and cubic structures, respectively. As a result, control of the crystallization temperature and dielectric properties can be realized by modulating the Pb and Sr content in the PSrT solid solution.[1,2]

Ferroelectric thin films mostly require low-temperature processes for integrated-circuit and microelectromechanical systems applications to prevent thermal damage of previously fabricated structure. Nevertheless, deposition of ferroelectric lead-titanate films, such as PTO and $Pb(Zr,Ti)O_3$ (PZT), are usually conducted at high temperatures (>600 °C) to achieve good crystallinity of a perovskite structure.[8] The high-temperature (>490 °C) process results in volatilizing lead oxide (Pb–O compounds) in lead-titanate-based thin films,[9,10] which in turn affects the film composition and degrades the electrical properties of the ferroelectric device. Thus, a low-temperature process with short thermal duration is certainly required for the deposition of PSrT thin films.

In this work, PSrT films were prepared on a $Pt/Ti/SiO_2/Si$ substrate at 200 °C using the pulsed-laser deposition (PLD) technique, and then the films were subjected to excimer laser annealing (ELA). The major advantages of the ELA technique are the formation of large grains with excellent structural quality and the ability to process selected areas. The noble metal platinum (Pt) is used as the electrode of the Pt/PSrT/Pt capacitor because of its low power consumption and low resistive capacitive delay,[6] compared to the conductive oxide.[9] The ELA technique can achieve local high-temperature heating within a very short duration, which has been applied in forming ultrashallow junctions[11] and producing low-temperature polysilicon thin-film transistors.[12–16] Some studies of the properties of PZT and $(Ba,Sr)TiO_3$ (BST) films post-treated by ELA have been reported.[17–21] However, the accumulated laser energy on physical/electrical properties of PSrT films has not been addressed much. Therefore, this study will investigate the effect of accumulated laser energy on the relationship between the structural and electrical characteristics of low-temperature-deposited (300 °C) PSrT films.

## II. EXPERIMENTAL PROCEDURES

A multilayer of $Pt/PSrT/Pt/Ti/SiO_2/p$-type Si was used to simulate the structure of a capacitor over a bit line. The

[a)]Electronic mail: yslai@nuu.edu.tw

TABLE I. Summarized material properties of PLD PSrT films nonirradiated and postexcimer laser annealed (post-ELA) at laser fluence of 47.6 mJ/cm$^2$ per pulse with various laser pulses.

| | | Number of post-ELA pulse | | |
|---|---|---|---|---|
| | Nonirradiated | 60 | 120 | 180 |
| rms surface roughness $R_{rms}$ (nm)[a] | 0.5 | 6.2 | 8.5 | 7.1 |
| $I_{100}$ (100)-oriented intensity[b] | 0 | 0 | 304 | 99 |
| $I_{110}$ (110)-oriented intensity[b] | 0 | 82 | 1081 | 392 |
| Pb/(Pb+Sr) lead elemental ratio[c] | 0.37 | 0.39 | 0.41 | 0.41 |
| Sr/(Pb+Sr) strontium elemental ratio[c] | 0.63 | 0.61 | 0.59 | 0.59 |
| Ti/(Pb+Sr) titanium elemental ratio[c] | 1.11 | 1.16 | 1.11 | 1.14 |
| O/(Pb+Sr) oxygen elemental ratio[c] | 2.83 | 2.84 | 2.89 | 3.07 |

[a]Evaluated from AFM analysis.
[b]Evaluated from GIAXRD pattern.
[c]Evaluated from ESCA analysis.

Pt/Ti films of 100/4 nm were sputtered onto the $SiO_2$/Si as the bottom electrode/adhesion layer. PSrT films 120 nm thick were deposited by a KrF pulsed-laser deposition (PLD) system (LPX 210i, Lambda Physik, $\lambda = 248$ nm, pulse width=25 ns). A set of optical lenses was used to focus the excimer laser beam onto the $(Pb_{0.6}, Sr_{0.4})TiO_3$ target. In the process of PLD PSrT film deposition, the target-to-substrate distance was 4 cm. The deposition temperature and oxygen pressure were 200 °C and 80 mTorr, respectively. The laser pulse rate and average laser fluence were 5 Hz and 1.55 J/cm$^2$ per pulse, respectively.

The position of the optical lens was changed in order to enlarge the irradiated area for laser annealing. The as-deposited PLD PSrT thin films were then postirradiated by the KrF excimer laser. The number of laser pulses was 60, 120, and 180. The laser fluence was controlled at

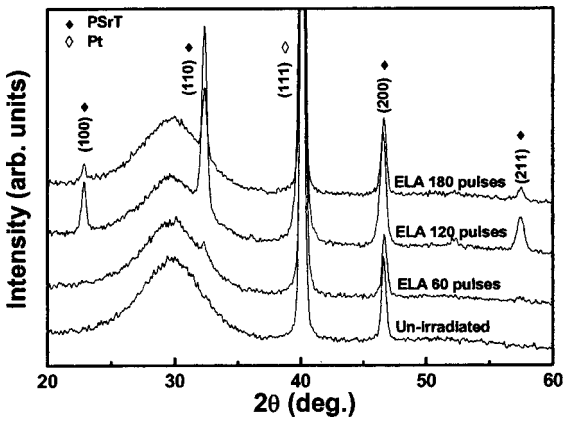


FIG. 1. Glancing-incident-angle x-ray diffraction (GIAXRD) patterns for PSrT films (a) nonirradiated and post-ELA with (b) 60, (c) 120, and (d) 180 pulses.

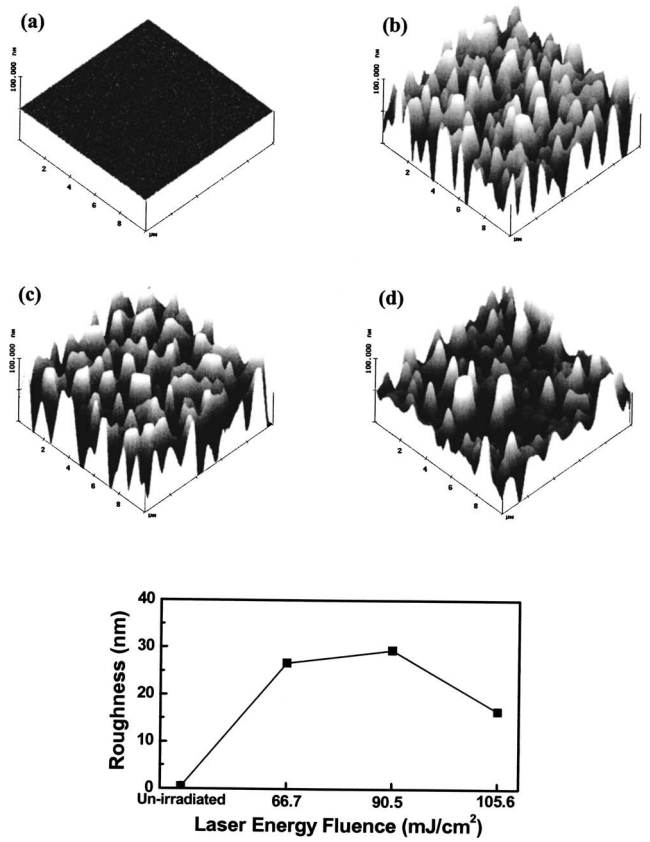


FIG. 2. [(a)–(d)] AFM images and (e) surface roughness of PLD PSrT films nonirradiated and postexcimer laser annealed (ELA) at various laser fluences: (a) nonirradiated, (b) 66.7, (c) 90.5, and (d) 105.6 mJ/cm$^2$.

47.6 mJ/cm$^2$ per pulse. To study the effect of the laser fluence, the number of laser pulses was kept at 40 pulses. The laser fluences are 66.7, 90.5, and 105.6 mJ/cm$^2$. The substrate temperature was 300 °C, which was calibrated at the wafer upper surface. Marmorstein *et al.* indicated that substrate heating would decrease the cooling rate of the temperature gradient induced by ELA, which would enhance the grain growth of ferroelectric films.[12] The oxygen pressure was fixed at 80 mTorr during the ELA process. The laser fluences were calibrated inside the vacuum chamber by a pyroelectric power meter.

The surface roughness of PSrT films was examined by atomic force microscopy (AFM) (DI Nano-Scope III, Digital Instruments). The stoichiometry of PSrT films was characterized by x-ray photoelectron spectroscopy [ESCA 210, Fison (VG)]. The crystallinity of the film was analyzed by glancing-incident-angle x-ray diffraction (GIAXRD) (D/MAX2500, Rigaku, using Cu $K\alpha$, $\lambda \sim 0.154$ nm) with a fixed incident angle of 2°. Cross-sectional transmission electron microscopy (TEM) samples were prepared by standard sample preparation techniques with tripod polishing and ion milling using the Gatan PIPS system operated at 3 kV. The TEM experiments were carried out on a JEM-2000FX (JEOL Ltd.) operated at 200 keV.

After the physical characterization, the Pt top electrodes, with a diameter of 165 $\mu$m, were deposited by sputtering and

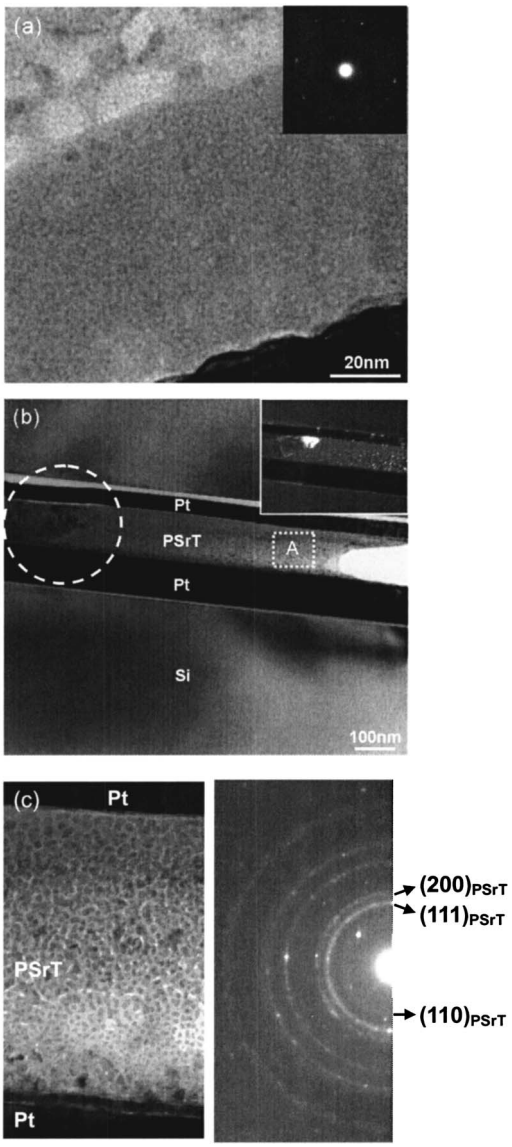


FIG. 3. Cross-sectional TEM images and selected-area diffraction patterns (SADPs) of PSrT films nonirradiated and post-ELA at laser energy fluence of 47.6 mJ/cm$^2$ per pulse with 180 pulses: (a) bright-field image and SADP of nonirradiated samples, (b) bright-field image and dark-field image (inset) of post-ELA samples, and (c) enlarged BF image and SADP (inset) of the square mark region.

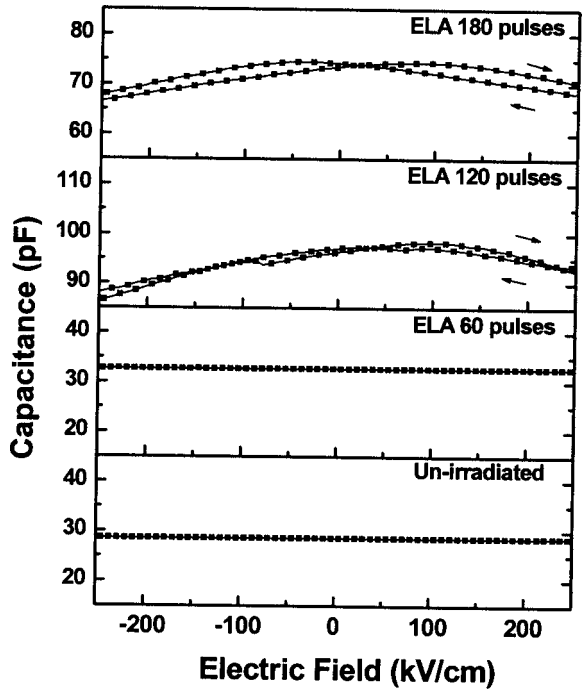


FIG. 4. Capacitance–electric field (*C-E*) hysteresis loops of PSrT films nonirradiated and post-ELA with various laser pulses.

were then patterned by the shadow-mask process. Next, the voltage was biased on the top electrode, and the bottom electrode was grounded. The combination of a semiconductor parameter analyzer (4156C, Agilent Technologies) and a probe station was used to measure the current-voltage (*I-V*) characteristics. A capacitance-voltage (*C-V*) analyzer (Package 82 system *C-V* 590, Keithley) was also used to measure *C-V* curves at 100 kHz.

## III. RESULTS AND DISCUSSION

To probe into the effects of ELA on PSrT films, the as-deposited sample was treated by mock-ELA with zero laser pulse (nonirradiated) to study the influence of substrate heating during the ELA process. Table I summarizes the physical properties of PLD PSrT films nonirradiated and postexcimer laser annealed (post-ELA) with various laser pulses. It can be seen that the minimum normalized root-mean-square roughness ($R_{rms}$) and maximum $R_{rms}$ are 0.5 and 8.5 nm for films nonirradiated and post-ELA with 120 pulses, respectively. The $R_{rms}$ further decreases as the number of laser pulses increases. Figure 1 shows the GIAXRD pattern of PSrT films as a function of laser pulses. The nonferroelectric pyrochlore phase is not observed from the GIAXRD pattern. The GIAXRD pattern presents the crystallinity of the upper region of PSrT films and indicates diffraction intensities of (100) and (110) orientations, which may be associated with the accumulated laser energy.[15,16] Table I also shows that the ratio of O to (Pb+Sr) [denoted by O/(Pb+Sr)] varies from 2.83 to 3.07 as the laser pulse increases. In contrast, the laser pulse seems to have little influence on the value of Pb/(Pb+Sr), Sr/(Pb+Sr), and Ti/(Pb+Sr). We infer that the oxygen deficiency on the surface of the films can be eliminated by increasing the total number of laser pulses. In short, these results suggest that the surface roughness, oxygen content, and crystallinity of the upper region of PSrT films could apparently be affected by increasing the number of laser pulses during ELA.

On the other hand, Fig. 2 shows AFM images of PSrT films before and after irradiation at various laser fluences. One can see that the surface roughness increases at first and then decreases as the laser fluence increases. In comparison, the surface roughness shows a similar trend to that of PSrT films irradiated with an increasing number of laser pulses.

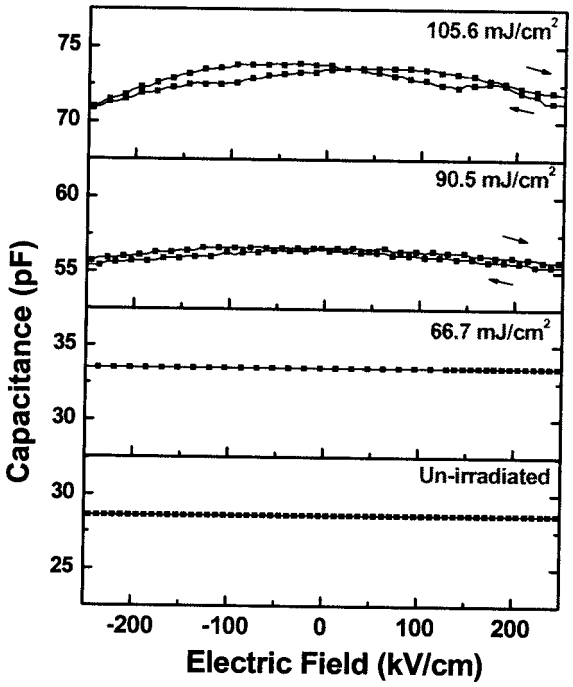


FIG. 5. Capacitance–electric field (*C-E*) hysteresis loops of PSrT films non-irradiated and post-ELA at various laser fluences.

The decrease of surface roughness is probably due to a melting state on the surface when irradiated with larger laser fluence or with more laser pulses.

Figure 3 shows the cross-sectional TEM images of PSrT films before and after irradiation with various laser pulses. The bright-field (BF) image of the non-irradiated PSrT film is shown in Fig. 3(a). Because of the lack of feature and no observed grain boundaries, we suggest that the nonirradiated PSrT film is amorphous. In addition, the corresponding selected-area diffraction pattern (SADP) [inset of Fig. 3(a)] with the diffuse ring pattern also confirms the amorphous state of the nonirradiated PSrT film. In contrast, the post-ELA film with 180 pulses reveals an image of a large reverse-pyramid grain [circular mark region in Fig. 3(b)] and numerous nanograins 2–5 nm in diameter, as seen in Fig. 3(b). The corresponding dark-field image is also shown in the inset of Fig. 3(b). The enlarged BF image with the square mark region in Fig. 3(b) is shown in Fig. 3(c). It clearly shows that the size of the nanograins decreases from film surface to the bottom, which suggests that most of the propagating laser energy is absorbed within the upper region of PSrT films. The corresponding SADP [inset of Fig. 3(c)] shows an intense ring pattern and indicates that the crystallinity of films is enhanced after the ELA treatment, consistent with the result of GIAXRD. The results show that grain growth induced by ELA is not uniform (i.e., from top to bottom of the film), and the influence of laser irradiation only works on the upper region of PSrT films. It indicates that only a few nanograins can grow into large grains, and most of the nanograins would repeat the process of coarsening, dissolving, and nucleating in each irradiation of the laser pulses, which was also observed in ELA polysilicon.[15,16]

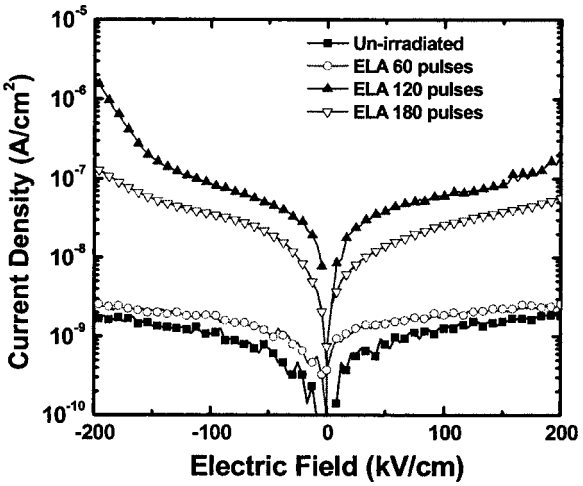


FIG. 6. Schottky emission plot fitting of $\log(J/T^2)$ vs $E^{1/2}$ for Pt/PSrT/Pt capacitors under (a) positive bias and (b) negative bias.

Figure 4 shows the capacitance versus electric field (*C-E*) characteristics of PSrT films as a function of laser pulses. The figure presents a typical *C-E* hysteresis characteristic of ferroelectric materials. According to the coercive field ($E_c$) of the hysteresis loop, the capacitance shows a maximum value at negative bias when the applied field sweeps from +200 to −200 kV/cm. However, the maximum capacitance appears at positive $E_c$ when the applied field sweeps in the reverse direction. It is argued that the asymmetric *C-E* loops may originate from the difference between the upper region and lower region of PSrT films, where the upper region is intensively impacted by ELA. The dielectric constants, evaluated from the zero-field capacitance, are 18.1, 20.7, 61.7, and 46.8 for films before and after ELA with 60, 120, and 180 pulses, respectively, which are consistent with the intensity of diffraction patterns. It indicates that the distinct *C-E* hysteresis loops and larger dielectric constants can be

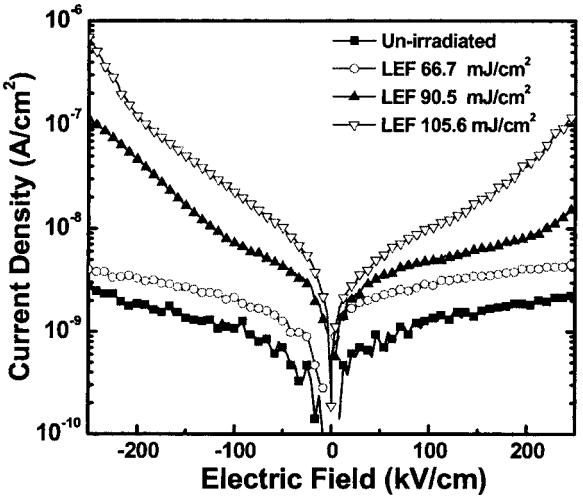


FIG. 7. Current density vs electric field (*J-E*) characteristics for PSrT films nonirradiated and post-ELA at various laser fluences.

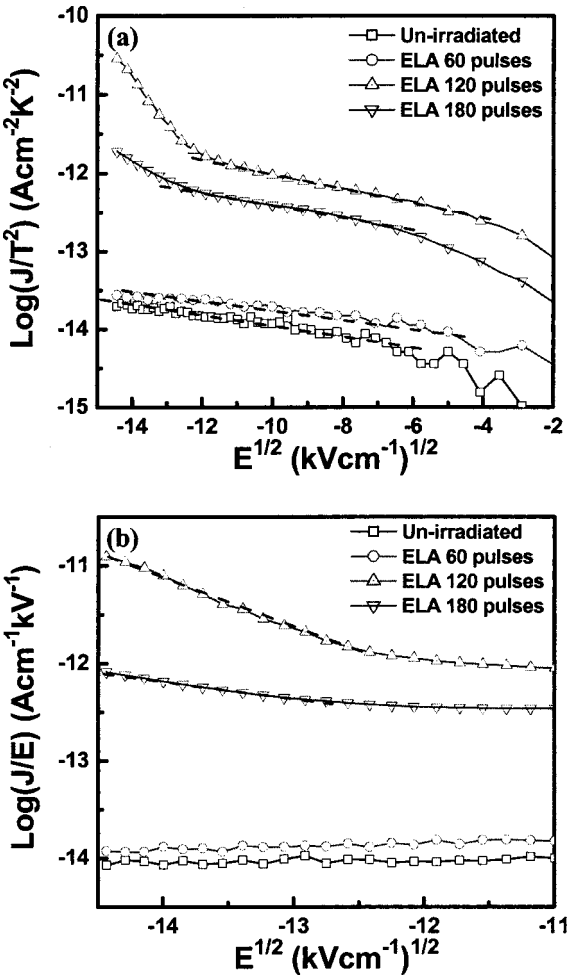


FIG. 8. Poole-Frenkel emission plot fitting of $\log(J/E)$ vs $E^{1/2}$ under negative bias for PSrT films nonirradiated and post-ELA with various laser pulses.

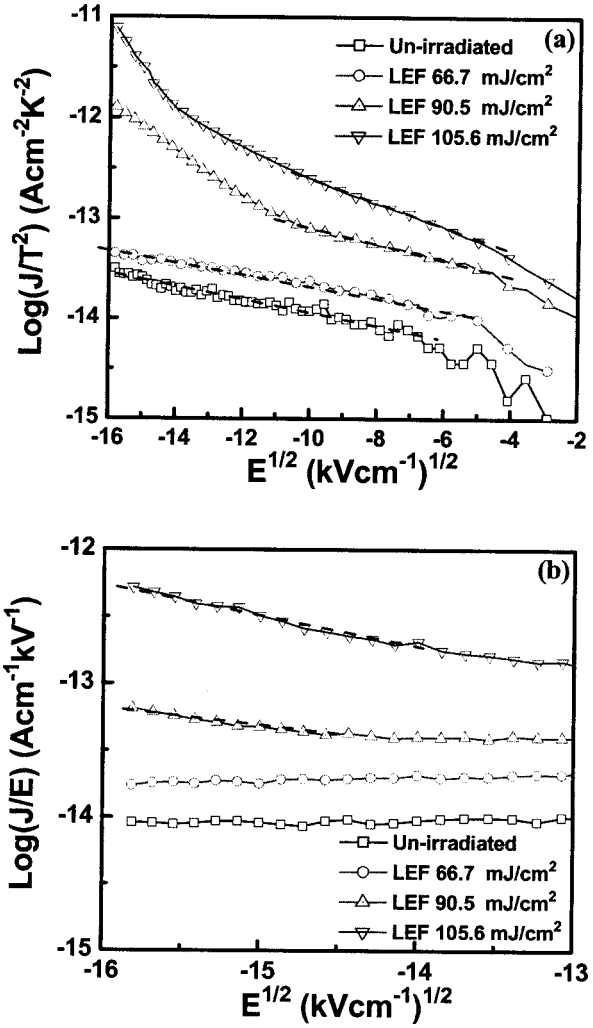


FIG. 9. (a) Schottky emission plot fitting of $\log(J/T^2)$ vs $E^{1/2}$ and (b) Poole-Frenkle emission plot fitting of $\log(J/E)$ vs $E^{1/2}$ for PSrT films nonirradiated and post-ELA at various laser fluences.

obtained by irradiating with more laser pulses ($\geqslant$120), which would improve the ferroelectricity of PSrT films.

Figure 5 shows the *C-E* characteristics of PSrT films as a function of laser fluence. The ferroelectricity appears when the laser fluence is higher than 90.5 mJ/cm$^2$. From Figs. 4 and 5, the results suggest that the ferroelectricity is improved by more laser pulses or larger laser fluences.

Figures 6 and 7 present the leakage current as a function of laser pulses and laser fluences. It is seen that the nonirradiated PSrT films exhibit the lowest leakage current. PSrT films irradiated with 120 pulses show the largest leakage current. On the other hand, the largest leakage current appears for films irradiated at 105.6 mJ/cm$^2$. It seems that the leakage current is associated with surface roughness, as shown in Table I and Fig. 2.

The conduction mechanism can be interpreted as Schottky emission (SE) and Poole-Frenkel emission (PF), where the trap states are related to interface-limited and bulk-limited characteristics, respectively.[18,22,23] If the conduction current follows SE behavior, then a $\log(J/T^2)$ against $E^{1/2}$ plot should be linear, where $T$ is the absolute temperature. Similarly, a $\log(J/E)$ against $E^{1/2}$ plot can be made for PF. Figures 8(a) and 9(a) present the SE plot of Pt/PSrT/Pt capacitors as a function of laser pulses and laser fluences, respectively. The leakage currents at low electric fields are dominated by the increased interface states, which strongly depends on laser pulses and laser fluences. The magnitude of the leakage current is usually associated with the oxygen stoichiometry and interfacial properties of ferroelectric films.[18,22] Since the conduction characteristics of PSrT films are mainly governed by SE at lower electric fields, the leakage current of films is most likely correlated with the interfacial properties. It is also observed that the asymmetry of leakage currents becomes significant as the laser pulses or laser fluences increase (Figs. 6 and 7). Since the materials of the top and bottom electrodes are the same (i.e., Pt), the increased leakage current under a negative bias can be linked to the defects at the upper electrode/film interface (i.e., the rough interface).[24,25] Figures 8(b) and 9(b) show the PF plot of Pt/PSrT/Pt capacitors as a function of laser pulses and laser fluences at high electric fields under negative bias. We found that the PF emission becomes the dominant conduction mechanism for films irradiated with more than 120 laser

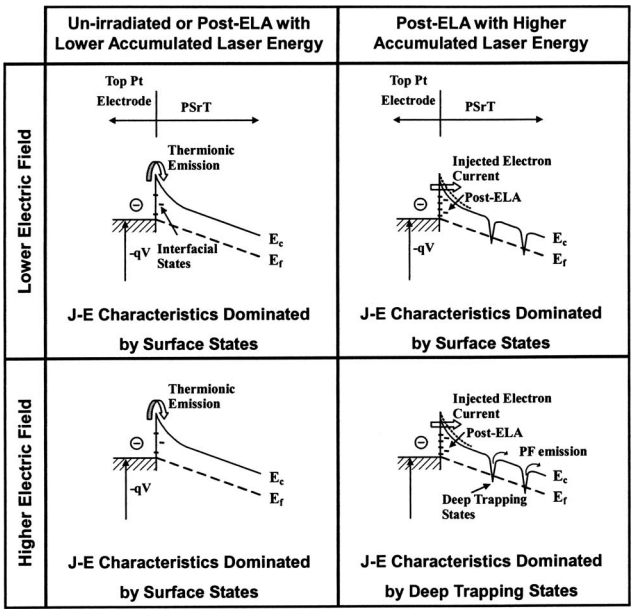


FIG. 10. Schematic drawings of the electron energy band for PSrT films with different accumulated laser energies.

pulses or with laser fluences larger than 90.5 mJ/cm$^2$. It implies that the deep trapping states are generated as the accumulated laser energy increases, which may be connected with the grain-boundary defects of the large grains induced by the ELA process (Fig. 3).

Figure 10 illustrates the electron energy band of PSrT films and shows that the interface of substrate electrodes acts as an *n*-type semiconductor due to the generation of oxygen vacancies in $ABO_3$ perovskites.[26] It reveals that PSrT films non-irradiated and post-ELA with fewer laser pulses ($<120$) or smaller laser fluences ($<90.5$ mJ/cm$^2$) have smoother surfaces and fewer surface defects, yielding the lower leakage current dominated by surface states and the conduction governed by SE behavior at the applied field range. Conversely, post-ELA PSrT films with more laser pulses ($\geqslant 120$) and larger laser fluences ($\geqslant 90.5$ mJ/cm$^2$) exhibit rougher surfaces, more surface defects, and deep trapping states inside films, yielding larger leakage currents. For post-ELA PSrT films with larger accumulated laser energy, the low-field leakage current is connected to the surface states and the high-field leakage current is mainly associated with deep trapping states, which suggests that conduction biased at a high-field state is attributed to PF behavior.

## IV. CONCLUSIONS

The effect of ELA on the material and electrical characteristics of PSrT films is investigated in this work. The intense diffraction ring from TEM indicates that the crystallinity of films is enhanced after the ELA treatment. It shows that ELA with more pulses results in larger grain sizes. However, the influence of laser irradiation only works on the upper region of films. The distinct *C-E* hysteresis loops and large dielectric constants are observed for films after ELA with 120 pulses, suggesting that the ferroelectricity could be improved with increasing the number of laser pulses. On the other hand, PSrT films after ELA with 180 pulses exhibit decreased dielectric constant and leakage currents, attributed to the reduced surface roughness. The conduction mechanism is mainly governed by SE for nonirradiated and irradiated films at low electric fields. However, the leakage current is dominated by PF at high electric fields for PSrT films irradiated with more laser pulses or larger laser fluences. The PF behavior at high electric fields is possibly due to the deep trapping states, which could be related to the grain-boundary defects induced by the ELA process.

## ACKNOWLEDGMENTS

This work was supported in part by the National Science Council of ROC under Contract No. NSC95-2221-E-009-253. Thanks are also due to the Nano Facility Center (NFC) in National Chiao Tung University and the National Nano Device Laboratory (NDL) of the NSC for technical support.

[1]D. H. Kang, J. H. Kim, J. H. Park, and K. H. Yoon, Mater. Res. Bull. **36**, 265 (2001).
[2]F. Zhang, T. Karaki, and M. Adachi, Jpn. J. Appl. Phys., Part 1 **44**, 6995 (2005).
[3]T. Karaki and M. Adachi, Jpn. J. Appl. Phys., Part 1 **44**, 692 (2005).
[4]C. C. Chou, C. S. Hou, G. C. Chang, and H. F. Cheng, Appl. Surf. Sci. **142**, 413 (1999).
[5]H. J. Chung and S. I. Woo, J. Vac. Sci. Technol. B **19**, 275 (2001).
[6]C. S. Hou, H. C. Pan, C. C. Chou, and H. F. Cheng, Ferroelectrics **232**, 129 (1999).
[7]G. Shirane and Y. Yamada, Phys. Rev. **177**, 858 (1969).
[8]D. Roy and S. B. Krupanidhi, J. Mater. Res. **7**, 2521 (1992).
[9]C. P. De Araujo, J. F. Scott, and G. W. Taylor, *Ferroelectric Thin Films: Synthesis and Basic Properties, Ferroelectric and Related Phenomena* (Gordon and Breach, Netherlands, 1996), Vol. 10, pp. 193–226 and 447–478.
[10]D. G. Lim, Y. Park, S. I. Moon, and J. Yi, Proceedings of the 12th IEEE International Symposium, Honolulu, 2000 (unpublished), p. 599.
[11]S. Whelan, A. La Magna, V. Privitera, G. Mannino, M. Italia, and C. Bongiorno, Phys. Rev. B **67**, 075201 (2003).
[12]A. Marmorstein, A. T. Voutsas, and R. Solanki, J. Appl. Phys. **82**, 4303 (1997).
[13]H. C. Cheng, C. C. Tsai, J. H. Lu, H. H. Chen, B. T. Chen, T. K. Chang, and C. W. Lin, J. Electrochem. Soc. **154**, J5 (2007).
[14]N. Matsuo, Y. Aya, T. Kanamori, T. Nouda, H. Hamada, and T. Miyoshi, Jpn. J. Appl. Phys., Part 1 **39**, 351 (2000).
[15]D. P. Gosain, A. Machida, T. Fujino, Y. Hitsuda, K. Nakano, and J. Sato, Jpn. J. Appl. Phys., Part 2 **42**, L135 (2003).
[16]M. He, R. Ishihara, W. Metselaar, and K. Beenakker, J. Appl. Phys. **100**, 083103 (2006).
[17]Y. Zhu, J. Zhu, Y. J. Song, and S. B. Desu, Appl. Phys. Lett. **73**, 1958 (1998).
[18]D. C. Shye, B. S. Chiou, C. C. Hwang, C. C. Jaing, H. W. Hsu, J. S. Chen, and H. C. Cheng, Jpn. J. Appl. Phys., Part 1 **42**, 1680 (2003).
[19]O. Baldus and R. Waser, J. Eur. Ceram. Soc. **24**, 3018 (2004).
[20]P. P. Donohue, M. A. Todd, and Z. Huang, Integr. Ferroelectr. **51**, 39 (2003).
[21]S. C. Lai, H.-T. Lue, K. Y. Hsieh, S. L. Lung, R. Liu, T. B. Wu, P. P. Donohue, and P. Rumsby, J. Appl. Phys. **96**, 2779 (2004).
[22]J.-L. Wang, Y.-S. Lai, B.-S. Chiou, H.-Y. Tseng, C.-C. Tsai, C.-P. Juan, C.-K. Jan, and H.-C. Cheng, J. Phys.: Condens. Matter **18**, 10457 (2006).
[23]A. Vorobiev, P. Rundqvist, K. Khamchahe, and S. Gevorgian, J. Appl. Phys. **96**, 4642 (2004).
[24]M. S. Tsai, S. C. Sun, and T. Y. Tseng, J. Am. Ceram. Soc. **82**, 351 (1998).
[25]N. Sugii and K. Tagagi, Thin Solid Films **323**, 63 (1998).
[26]J. F. Scott, *Ferroelectric Memories* (Springer, Berlin, 2000), pp. 79–85 134–143.